Nanoscale

PAPER

View Article Online
View Journal | View Issue

Cite this: *Nanoscale*, 2026, **18**, 9756

Comparison of magnetic nanoparticle immobilization methods using MPS and MRX

Kerstin Pansegrau, *[a,b,c] Patricia Radon, [c] Aaron Jaufenthaler, [b] Frank Wiekhorst [c] and Daniel Baumgarten [b]

Magnetic nanoparticles (MNP) are employed in many technical and clinical applications for which the knowledge of their magnetic properties is mandatory. This comprises not only the intrinsic magnetic parameters, but especially in biomedical applications the changes of the MNP behavior in a certain environment or binding state such as the immobilization of the MNP after cellular uptake, blood contact or injection into tissue. Therefore, the magnetic properties of MNP samples that have been immobilized are considered to mimic the binding of MNP to human tissue. However, the procedure and materials used for immobilization differently impact their magnetic properties. Here, we investigated common immobilization methods regarding reproducibility and variation in terms of the magnetic properties of the commercial nanoparticle system perimag® for the three available surface coatings. We considered immobilization by polyacrylamide embedding, freeze drying, gypsum crystallization, filter paper as well as cotton wool drying. We used the two magnetic measurement techniques magnetic particle spectroscopy (MPS) and magnetorelaxometry (MRX) to assess the magnetic properties and changes thereof for all immobilization methods. We found highest reproducibility and less variation in magnetic parameters for freeze dried and gypsum immobilization. A higher variation of magnetic properties was observed for evaporation-based methods filter paper and cotton wool attributed to unstructured arrangement of MNP on the fibers of the immobilization materials. The surface modification of the MNP system shows a minor impact on immobilization procedure. From our results, we deduce recommendations and practicability considerations for immobilization methods in preparation and handling of MNP reference samples.

Received 16th December 2025,
Accepted 11th March 2026

DOI: 10.1039/d5nr05283a

rsc.li/nanoscale

1. Introduction

Magnetic nanoparticles (MNP) have become an important constituent in a number of medical applications such as magnetic resonance imaging,[1,2] magnetic particle imaging (MPI),[3] magnetorelaxometry (MRX),[4,5] magnetorelaxometry imaging (MRXI),[6–8] magnetic drug targeting[9] and magnetic hyperthermia.[10] Not only for these clinical application scenarios but also for technical applications of MNP such as sensing,[11] the characterization of MNP is essential.

Often the characterization of structural and magnetic properties is carried out with MNP in solutions, *i.e.* the MNP are suspended in a liquid. Although this might be appropriate for basic magnetic characterization of an MNP system, it often does not reflect the situation of the MNP in the biomedical application. In magnetic hyperthermia, for instance, the MNP are injected directly into a body tissue, leading to their partial immobilization.[5,12–14] Similarly, the MNP are embedded after cellular uptake inside the lysosomes of cells leading to immobilization and aggregation of MNP changing the magnetic properties of the MNP.

Therefore, experiments to assess the capability of an MNP system in a biomedical application are carried out using immobilized MNP samples. Such reference samples, in combination with defined procedures, allow a more appropriate characterization of MNP behavior in the underlying biomedical application. For this, different immobilization mechanisms are commonly used, such as embedding in a crystal matrix (sugar by freeze drying, $CaSO_4$ in gypsum crystallization), incorporation into a non-magnetic polymer, or drying on a carrier material (paper, cotton wool) by evaporation of the carrier liquid.

Whereas MNP immobilization in gypsum[15–17] and by freeze drying[5,18,19] is rather common, other immobilization materials such as silicon,[20] absorbent cotton,[21] filter paper,[22] epoxy resin[23] and photopolymer[24,25] are occasionally chosen. In addition to these immobilization materials with low similarity

[a]*Institute of Electrical and Biomedical Engineering, UMIT TIROL – Private University for Health Sciences and Health Technology, Hall in Tirol, Austria.*
E-mail: Kerstin.Pansegrau@umit-tirol.at
[b]*Biomedical Engineering Group, Department of Mechatronics, University of Innsbruck, Innsbruck, Austria*
[c]*Physikalisch-Technische Bundesanstalt, Berlin, Germany*

to human tissue, hydrogels are produced with MNP embedded in gelatine,[13,26–28] agarose,[29,30] polyacrylamide[31,32] and bovine serum albumin.[28] Although hydrogels are often not produced purely for the purpose of MNP immobilization alone, they are assumed to resemble MNP in cells to a greater extent.[33] In general, reference samples are superior in terms of storage conditions compared to biological samples made from cells and tissues, as they do not age the way biological samples do[34] and do not need to be regularly supplied with nutrient media. This makes them particularly advantageous for early-stage experiments.

Most studies are performed with one or at most two immobilization methods.[35–37] Nevertheless, the results of these studies are often related to immobilized MNP in general. This generalization is rarely appropriate because the diversity of immobilization methods suggests different magnetic properties of the obtained reference samples. It is reasonable that the immobilization materials trigger different chemical mechanisms of MNP embedding and interact differently with the various MNP systems, *i.e.* due to their varying surface functionalities and size distributions. Combined with different immobilization speeds and MNP system dependent aggregation probabilities,[19] variations of the three-dimensional arrangement of MNP in the immobilization material are likely and would lead to variations of the samples' magnetic properties. Whereas a number of studies have been presented for the comparison of the magnetic properties of suspended and immobilized MNP,[37] there are only a few investigations on the differences between immobilization methods, with a focus on biological media,[19,28,38] hydrogels[13,28] and *ex vivo* tissues.[13,28] No systematic comparison of the frequently used immobilization methods that are less similar to human tissue, such as gypsum or freeze drying, has yet been carried out.

In addition to the differences between immobilization methods, variations in the magnetic properties within a method are expected because the production of samples involves several steps that are prone to different degrees and kinds of uncertainties. Immobilization processes with more and error-prone steps should result in higher variability, *i.e.* lower reproducibility of the magnetic properties. Furthermore, it can be assumed that the manifestation of MNP interactions varies between reference samples of the same immobilization type. However, a single immobilized sample has been prepared for most experiments,[36,37] and no statements are made about the variability of the investigated aspects within the chosen immobilization method.

For investigating both, the influence of the immobilization method on the magnetic properties of reference samples and the reproducibility of the magnetic properties within each immobilization method, the well-established modalities magnetic particle spectroscopy (MPS)[3,38] and MRX[14,19,39] are particularly suitable. In MPS, the MNP are exposed to a sinusoidal oscillating magnetic field and the non-linear dynamic magnetic response is analyzed in the frequency domain. In contrast, MRX uses a DC excitation field to magnetize the MNP and measures the relaxation signals in the time domain after the excitation field is switched off as the decaying stray field of the MNP with Superconducting Quantum Interference Device (SQUID) sensors[14,40] or Optically Pumped Magnetometers (OPMs).[36] Both measurement modalities provide signal parameters that directly form the basis for the MNP-based imaging modalities MPI and MRXI. The detailed investigation of the influence of immobilization on these MPS and MRX signal parameters thus offers particular potential for directly improving application-related research.

In this work, the influence of common non-biological immobilization methods on the magnetic properties of MNP reference samples is systematically investigated for the first time. For this purpose, samples are produced employing three differently coated commercially available MNP systems and six immobilization methods. Five replicates are prepared for each combination and their magnetic properties are examined using MPS and MRX. This also allows, for the first time, a detailed investigation of the reproducibility of the magnetic properties within the immobilization methods. Keeping the iron amount the same for all samples we could derive the changes as detected by MPS and MRX due to the immobilization process in relation to the magnetic behavior of suspended samples. Since the magnetic properties of (immobilized) MNP are the leading characteristic for (clinical) applications, this study focuses exclusively on the immobilization-related effects on magnetic properties rather than examining the material effects responsible for them in detail. Following the description of the methodology, the results of the two measurement modalities are first presented and described before being discussed as a whole. The results are used to derive recommendations regarding the selection of immobilization methods and the handling of the corresponding reference samples.

2. Materials and methods

2.1. MNP systems and characterization

Perimag® nanoparticles (micromod Partikeltechnologie GmbH, Germany) with all three available surface functionalities were included in this study, namely perimag® COOH, perimag® NH2 and perimag® plain. The MNP systems are abbreviated as COOH, NH2 and plain in the following. Basic information on the systems used can be found in Table 1.

The main structural and magnetic properties of the chosen MNP systems were characterized prior to immobilization. For structural characterization, the size distribution, the mean hydrodynamic diameter and the polydispersity index (PDI) of six repetitive measurements were determined based on the standard cumulants approach[41] with the Zetasizer Nano ZS (Malvern Panalytical, UK). The mean zeta potential, reflecting the effective surface charge of the MNP, including standard deviation, was determined from 52 repetitions by dynamic light scattering (DLS, Zetasizer Nano ZS, Malvern Panalytical, UK). The iron concentration of the MNP solution in the target

Table 1 Information on the three perimag® stock suspensions included in the study

MNP system	Product code	Lot number	Measured stock iron concentration (mmol L^{-1})	Nominal hydrodynamic diameter (nm)
COOH	102-02-132	03224102-02	87.8	130
NH2	102-01-132	02924102-01	91.4	130
Plain	102-00-132	03724102-08	155.0	130

dilution was determined photometrically (SpectraMaxPlus384, Molecular Devices, USA).

The magnetic properties of the three MNP systems were investigated by DC-magnetization (DCM) and linear AC-susceptibility[42] (ACS) measurements. For the DCM measurement, one sample for each MNP system (V = 50 μL, c(Fe) = 5 mmol L^{-1}) was prepared by freeze drying. The samples were measured with a commercial SQUID magnetometer (MPMS-XL, Quantum Design, USA) at T = 295 K in the magnetic field range B = ±5 T. The resulting magnetization curve $M(H)$ reflects the size and anisotropy (distribution) of the MNP system. The magnetization curve is normalized to the total amount of iron in the sample leading to the (mass) magnetization $M(H)$ (in units of Am^2 $kg(Fe)^{-1}$). A linear diamagnetic background contribution from the sample container was subtracted and then the saturation magnetization $M_S = M(H = 4 \times 10^6$ A $m^{-1})$ was determined from the experimental data as the magnetization value at the highest applied magnetic field.

Room temperature (T= 295 K) ACS measurements of the three MNP systems were carried out to assess the hydrodynamic size distribution using a commercial AC susceptometer (DynoMag, RISE Acreo, Sweden). For the measurements, a quartz glass cuvette was filled with a sample volume of 200 μL MNP suspension, and χ' and χ'' parts of the magnetic susceptibility were acquired in the frequency range of 1 Hz to 100 kHz at an excitation amplitude of 0.2 mT. The initial mass susceptibility χ_0 (in units of m^3 $kg(Fe)^{-1}$, normalized to the sample iron mass) was obtained by extrapolation of the real part susceptibility χ' to frequency f = 0 Hz.

2.2. Choice of immobilization methods

We employed six commonly used immobilization methods: freeze-drying, gypsum, filter paper, absorbent cotton (referred to as cotton), synthetic absorbent cotton (referred to as synthetic cotton) and 5%-polyacrylamide. Due to thermal instability and preparation issues, MNP immobilization in gelatine and agarose were excluded. MNP diluted in distilled water to c(Fe) ≈ 10 mmol L^{-1} (referred to as suspended) were included for comparison.

2.3. Reference sample preparation

To prepare the MNP samples, the stock suspensions of the MNP systems were diluted with distilled water to an iron concentration of c(Fe) ≈ 10 mmol L^{-1}. Since the same volume of the diluted MNP systems is used for all reference samples, all samples of the three MNP systems contained the same amount of iron. For each MNP system, five individual suspended sample replicates of 10 μL volume were pipetted directly from the MNP dilution into target sample containers (PCR cups). In addition, five replicates were produced for each combination of MNP system and immobilization method according to the following protocols.

2.3.1. Freeze dried samples. 10 μL of the MNP dilution and 10 μL of 10%-Mannitol solution was pipetted into the PCR cup and mixed with the pipette. The subsequent freeze drying was performed over night (Alpha 1–4 LSC, Martin Christ Gefriertrocknungsanlagen GmbH, Germany).

2.3.2. Gypsum samples. 10 μL MNP dilution was pipetted into the PCR cup to which about 50 mg gypsum powder (Moltofill, Akzo Nobel Deco GmbH, Germany) was added. Then, the container was left open for at least 12 hours during crystallization of the gypsum at room temperature.

2.3.3. Filter paper samples. Two holes were punched from a commercial coffee filter (recycled paper), placed into the PCR cup and pressed into the center with a tweezer so that the edges were facing upwards. 10 μL of the MNP dilution was pipetted on top and the cup was left open over night for water evaporation at room temperature.

2.3.4. Cotton and synthetic cotton samples. A tweezer tip full of absorbent cotton (100% organic cotton, from cotton buds) or synthetic absorbent cotton (medical, from wound pad) was placed in the tip of the PCR cup. 10 μL of the diluted MNP was pipetted onto the cotton. The containers were left open over night for water evaporation at room temperature.

2.3.5. Polyacrylamide samples. For each MNP system, a 500 μL batch of 5%-polyacrylamide was prepared with the MNP dilution factors given above. Components and their volumes are shown in Table 2. The pipetting was performed in an ice bath under the fume hood. For each sample, 10 μL of the non-polymerized batch was pipetted into a PCR cup. The

Table 2 Components and volumes for the three 5%-polyacrylamide batches (one for each of the three MNP systems perimag® plain, COOH and NH2)

Component	Volume (μL)		
	For plain	For COOH	For NH2
Acrylamide 30%	83	83	83
Bisacrylamide 2%	81	81	81
Distilled water	288	258	265
Ammonium persulfate 10%	14	14	14
MNP stock suspension	33	63	56
Tetramethylethylenediamine 99.9%	1	1	1

containers were closed and stored in the refrigerator over night.

Alongside the polyacrylamide reference samples, six additional samples were cut out of each of the left over polymerized batches and weighed to about 10 mg in order to check homogeneity (referred to as cut polyacrylamide). The first two pieces were cut out from the top slice of the batch, pieces 3 and 4 were taken from the middle slice and the last two pieces from the bottom slice of the batch.

For each set of identically prepared samples (except cut polyacrylamide), one control sample was produced by following the same protocol but using distilled water instead of the MNP dilution. All sample containers were closed and at room temperature before the MPS and MRX measurements. The reference sample preparation and all measurements were carried out at Physikalisch-Technische Bundesanstalt (PTB, Berlin, Germany).

Table 3 summarizes the characteristics of the preparation procedures for all tested reference samples.

2.4. MPS analysis

MPS measurements of the samples were performed one day after their preparation using a commercial magnetic particle spectrometer (MPS-3, Bruker Biospin, Ettlingen, Germany) operating at an amplitude B_{ex} = 25 mT and a frequency f_0 = 25 kHz. The temperature inside the MPS device was kept at approximately 302 K during the measurements. For measurement, a fast reaction tube (Applied Biosystems®, MicroAmp, ThermoFischer, Schwerte, Germany) containing a sample volume of 10 μL was placed in the detection coil system of the MPS system. The induced magnetization response was acquired and averaged over an interval of 10 s. After Fourier transform of the time response signal, the spectral components of an MPS measurement are obtained, showing distinctive amplitudes A_i at odd multiples (odd harmonics i = 3,5,7,...) of the excitation frequency f_0. From all MPS spectra, a background measurement was subtracted, increasing the signal to noise factor by about two orders of magnitude. In order to determine the background signal variation, 25 MPS measurements were carried out with an empty PCR cup from which the tripled standard deviation was calculated. For the graphical representation of the MPS spectra, only the odd harmonics 3 to 39 were considered, as higher harmonics made no contribution distinguishable from the background signal.

Commonly, three parameters of the MPS spectra are used to characterize the general dynamic magnetic behavior of an MNP system: the amplitude of the third harmonic (A_3), the ratio between 5th and 3rd harmonic (A_5/A_3), and the phase of the 3rd harmonic (ϕ_3). All parameters are sensitive to changes in mobility and binding state due to the local MNP environment.[43] The parameter A_3 depends on the absolute MNP amount of the sample and is often used for MNP quantification in application.[44] For iron oxide MNP systems A_3^* is computed by normalizing A_3 to the iron amount of the sample according to eqn (1),

$$A_3^* = \frac{A_3}{c(\mathrm{Fe})_{\mathrm{MNP}} \cdot V_{\mathrm{MNP}} \cdot M(\mathrm{Fe})} \quad (1)$$

where $c(\mathrm{Fe})_{\mathrm{MNP}}$ is the iron concentration of the corresponding MNP system in target dilution (*cf.* Table 4). V_{MNP} = 10 μL is the volume of the MNP dilution within the reference sample and M(Fe) = 55.845 g mol^{-1} is the molar mass of iron. The A_3^* value still depends on the actual iron amount in each sample (*i.e.* MNP amount dependent). Parameters A_5/A_3 and ϕ_3 are extracted directly from the MPS spectra. The influence of the

Table 4 Results of characterization of the three included perimag® MNP systems

Property	COOH	NH2	plain
Mean hydrodynamic diameter (*Z*-average) (nm)	109.0	191.1	114.6
Polydispersity Index (PDI) (unitless)	0.203	0.130	0.167
Iron concentration (mmol L^{-1})	11.2	9.7	9.4
Zeta potential ± standard deviation (mV)	−33.20 ± 8.42	27.90 ± 7.12	−3.26 ± 6.55

Table 3 Characteristics of the preparation process for the MNP immobilization methods (suspended sample is shown for comparison purposes)

	Reference sample					
Characteristic	Polyacrylamide[31,32]	Freeze drying[5,18,19]	Gypsum[15–17]	Filter paper[22]	(Synth.) cotton[21]	Suspended
Main mechanism responsible for immobilization	Polymerization	Crystallization	Crystallization	Evaporation	Evaporation	—
Similarity to MNP-loaded tissue	Medium	Low	Low	Low	Low	Low
Number of preparation steps	8	4	3	3	3	2
Number of ingredients	6	3	3	3	3	2
Accuracy of quantities of immobilization materials	High	High	Medium	Medium	Medium	High
Complexity of required equipment	High	Medium	Low	Low	Low	Low
Approx. time for sample preparation (min)	20	3	3	3	3	1
Approx. time until complete immobilization (h)	0.25	6	0.25	20	20	—

actual amount of iron in each sample cancels out for these parameters due to their relative character (*i.e.* MNP amount independent). For all three MPS parameters, mean value, standard deviation and coefficient of variation (CV; percentage ratio of standard deviation to mean value) were calculated over the samples of each immobilization method. To assess the homogeneity of MNP embedding in polyacrylamide samples, A_3^* was normalized to the individual total mass of the polyacrylamide MNP sample denoted by the parameter $\tilde{A}_3^*$.

2.5. MRX analysis

MRX measurements were performed using a SQUID-based six-channel setup at PTB.[45] The samples were magnetized in a magnetic field of H = 2.15 kA m^{-1} (B = 2.7 mT) for one second. The SQUID channel (#4) located directly below the sample ($d \approx$ 13 mm) was selected as it provides the highest signal amplitude. Relaxation signals were recorded for 0.51 s at a sampling frequency of 100 kHz. All MRX measurements were carried out in triplicate at sample temperature T = 273 K. Background MRX measurements with empty sample holder were subtracted to increase the signal to noise ratio.

From recorded MRX signals, the three characteristic parameters relaxation amplitude ΔB, relaxation time $t_{1/e}$ and integral relaxation time IRT were extracted. ΔB is directly proportional to the MNP amount facilitating MNP quantification in biomedical applications.[46] The other two parameters, $t_{1/e}$ and IRT, characterize the shape of the MRX curve and are independent of the iron amount and therefore less prone to preparation inaccuracies. To obtain the MRX parameters, the background signal and the individual offset (mean signal amplitude of the last 20 ms) were subtracted for all MRX shots. Next, the relaxation signal was fitted to a sum of ten exponential functions using Orthogonal Matching Pursuit[47] (OMP, dictionary of 25 exponential functions, time constants between 0.1 s and 1.5 s) according to eqn (2),[16]

$$B^{\mathrm{fit}}(t) = B_0 + \sum_{n=1}^{10} B_n e^{-t/\tau_n} \tag{2}$$

where $B^{\mathrm{fit}}(t)$ refers to the fitted relaxation signal, B_0 refers to the offset component of the fit, B_n refers to the amplitude of exponential function n and τ_n refers to its time constant. The three fitted relaxation shots for one reference sample were averaged before the relaxation amplitude was computed according to eqn (3),

$$\Delta B = B^{\mathrm{fit,avg}}(t_1) - B^{\mathrm{fit,avg}}(t_2) \tag{3}$$

where $B^{\mathrm{fit,avg}}(t_1)$ and $B^{\mathrm{fit,avg}}(t_2)$ are the magnetic flux densities of the fitted and averaged relaxation signal at time points t_1 = 40 ms and t_2 = 300 ms, respectively. Fig. 1 shows the raw data and fitted relaxation signals for six measurements of the same sample (perimag® plain in polyacrylamide, repeated sample insertion) carried out to determine the procedural uncertainty for MRX. For the homogeneity check with the cut polyacrylamide samples, ΔB was normalized to the individual mass of each polyacrylamide piece leading to the parameter $\widetilde{\Delta B}$. The relaxation time was computed according to eqn (4),

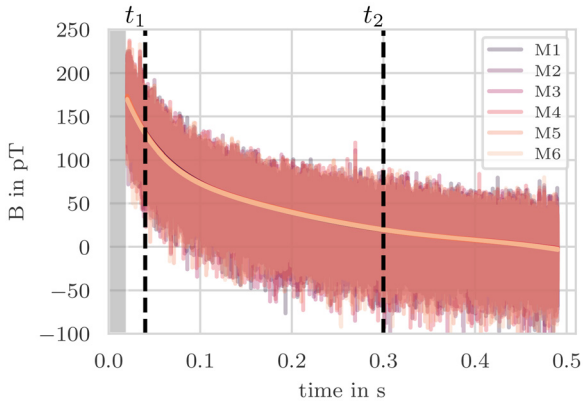

Fig. 1 Relaxation signals of a perimag® plain MNP sample immobilized with polyacrylamide measured six times (color coded). The broad transparent signals represent the raw data, whereas the solid lines represent the corresponding fitted signals. Please note that the variation of the fitted signals is within the linewidth of the displayed curve. The excitation field is turned off at t = 0 ms. The dashed vertical black lines indicate the time points t_1 = 40 ms and t_2 = 300 ms used to determine the MRX parameters. The beginning of the measurement signal contains a short section after the excitation current is switched off, which is not evaluated due to switching effects (dead time, gray background).

$$t_{1/e} = t\left(\frac{1}{e} B^{\mathrm{fit,avg}}(t_1)\right) - t_1 \tag{4}$$

and corresponds to the time in which the signal amplitude $B(t)$ has dropped to $1/e$ of its initial value at t_1. For obtaining IRT, the fitted relaxation curve was normalized to values between one and zero before its integral is approximated by the Riemann sum (midpoint rule). The IRT reflects shape variability of relaxation curves.

The mean value, standard deviation and CV of each MRX parameter were computed for each immobilization method.

3. Results

3.1. MNP characterization

3.1.1. Structural characterization. The results of the structural characterization are shown in Table 4 and Fig. 2 (size distributions). Whereas the mean hydrodynamic diameter for COOH and plain is found to be in the range of the manufacturer's specification (130 nm), a significantly larger mean hydrodynamic diameter (191.1 nm) and a shifted size distribution towards larger hydrodynamic diameters is observed for the NH2 system. The PDIs obtained for all MNP systems are in a similar range. The photometric determination of the iron concentration of the diluted MNP systems confirms similar iron concentrations for all samples in this study, *i.e.* iron amounts of 6.3 µg, 5.4 µg and 5.3 µg for 10 µL diluted COOH, NH2 and plain, respectively. The mean effective electrical charge of the MNP' surfaces (average zeta potential) is clearly

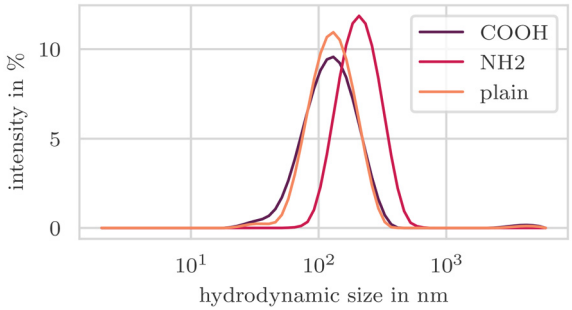

Fig. 2 Averaged distribution of hydrodynamic diameters (sizes) according to intensity for the three perimag® MNP systems (color coded) obtained from six DLS measurements each.

positive for NH2 and clearly negative for COOH. A slightly negative zeta potential can be observed for plain, but this remains within a single standard deviation.

3.1.2. Magnetic characterization of the initial MNP systems. The results of the DC magnetization measurements are shown in Fig. 3. All three MNP systems exhibit nearly identical $M(H)$ behavior approaching the same saturation magnetization value of about M_S = 89 Am^2 $kg(Fe)^{-1}$ and exhibiting no significant hysteresis (*cf.* Fig. 3). This is typical for a multi-core MNP system, where due to the small particle size of the individual crystallites forming the multi-core particle, the majority of the magnetic moments are not thermally blocked at T = 295 K. For the DCM measurements, a measurement uncertainty of about 3% is estimated (1% contribution from the measurement device, 2% due to preparation and the iron concentration determination).

The real (in-phase) χ' and imaginary (out-of-phase) parts χ'' of the complex dynamic (mass) susceptibility for the three systems are displayed in Fig. 4. The two coated systems show a very similar behavior with an initial susceptibility of χ_0 = 0.02 m^3 $kg(Fe)^{-1}$ whereas the plain system displays an

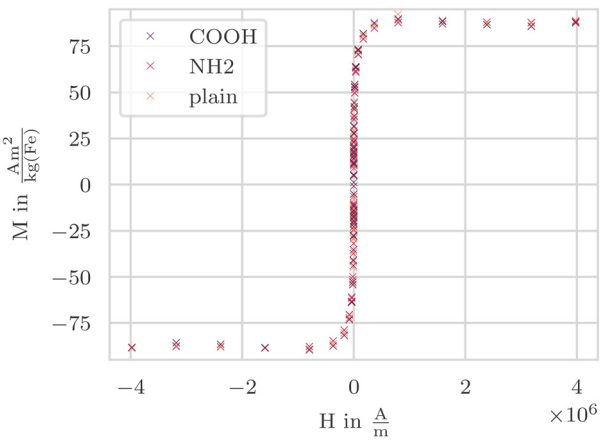

Fig. 3 Room temperature (T = 295 K) DC magnetization curves of the three perimag® systems COOH, NH2, and plain in the immobilized state (freeze dried). For graphical representation a linear, diamagnetic contribution resulting from the sample container has been subtracted.

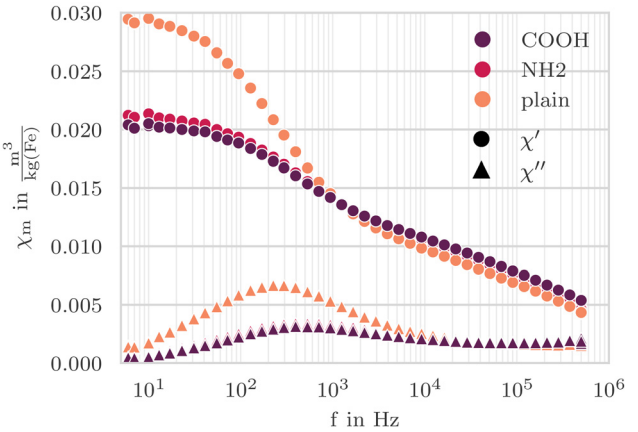

Fig. 4 Room temperature (T = 295 K) ACS measurements of the three perimag® systems plain, COOH, and NH2 (color coded) in the suspended state. The circles denote the real part, the triangles the imaginary part of the complex dynamic susceptibility.

additional susceptibility contribution for f < 1 kHz leading to a significantly higher χ_0 = 0.03 m^3 kg(Fe). Above that frequency, the complex dynamic susceptibility is nearly identical for all three MNP systems. All three systems exhibit a broad maximum in χ'' which corresponds to a (mean) effective relaxation time τ of the MNP where $\omega\tau \approx 1$. For the ACS measurements, an overall measurement uncertainty of about 4% is estimated (2% contribution from the measurement device, 2% due to preparation and iron concentration determination).

3.2. MPS analysis

3.2.1. Magnetic impurities of immobilization materials. Fig. 5 shows the mean background signal of the empty sample container as well as the MPS spectra for the control samples (immobilization material with distilled water instead of MNP dilution). The mean background signal observed is $(4.8 \pm 2.4) \times 10^{-12}$ Am^2 for the third harmonic and decreases to $(2.8 \pm 1.0) \times 10^{-13}$ Am^2 for the 39th. For gypsum (s. Fig. 5(d)), clear contributions above the background signal can be seen up to the 21st harmonic. A contribution above the background signal is also visible for the third harmonic of the filter paper spectra (s. Fig. 5(e)) and less pronounced for all other immobilization methods. Above, the signals are in the same range as the background signal, respectively.

3.2.2. Influence of immobilization method on MPS spectra. Fig. 6 presents the MPS spectra for the different immobilization methods, exemplarily for the plain particles. Regarding the shape of the spectra, two basic types can be distinguished: particles that are suspended (s. Fig. 6(a)) or immobilized with crystallization-based or polymerization-based methods (s. Fig. 5(b)–(e)) show a gently declining spectrum with contributions clearly above the background signal up to A_{39}. In contrast, particles immobilized with evaporation-based methods show a steeper drop in the contributions of lower harmonics, whereby the signal is already at background signal level from the 23rd (filter paper, cotton, s. Fig. 5(f) and

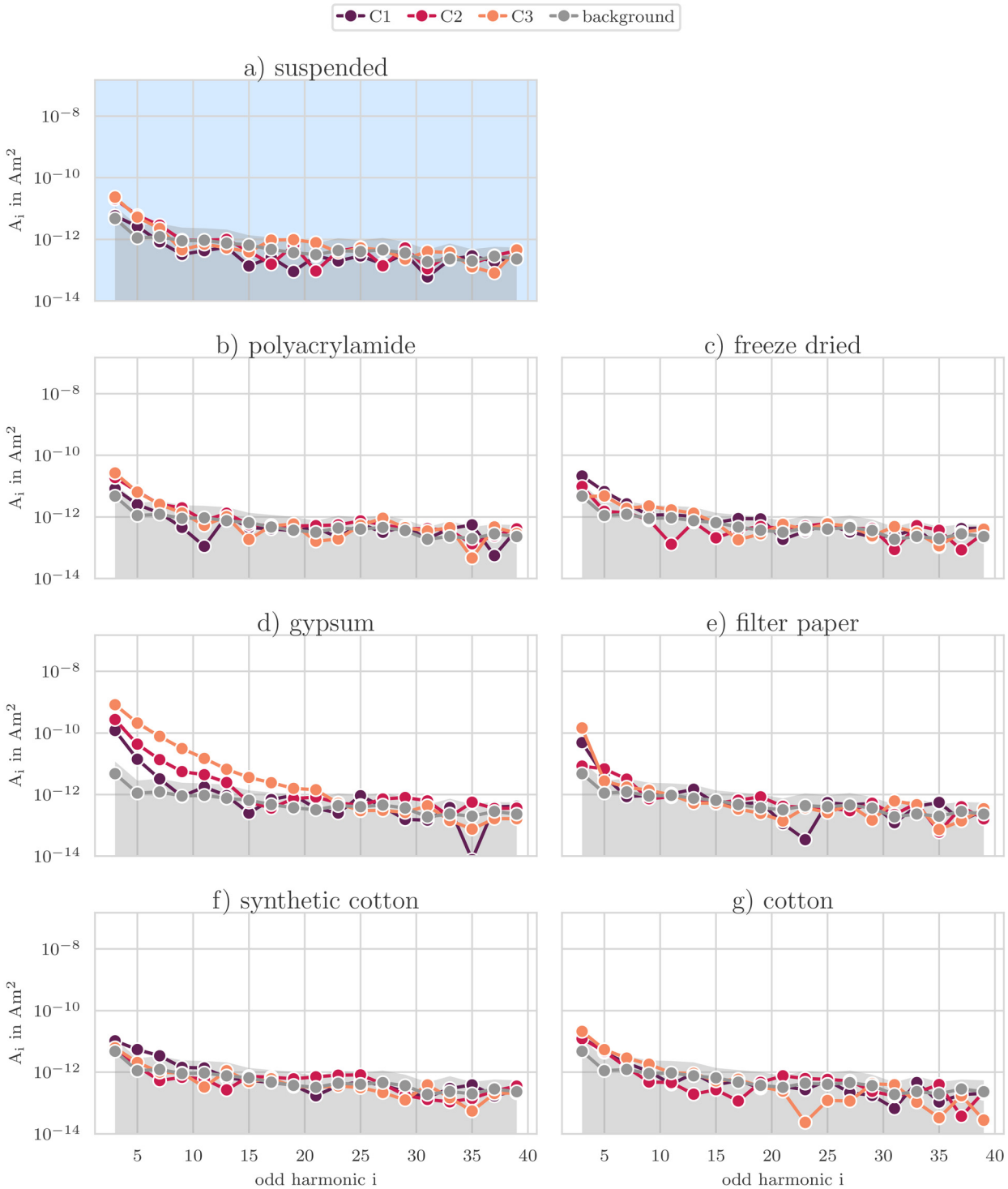

Fig. 5 MPS spectra of control samples (distilled water without MNP). Shown are the odd harmonics for three replicate samples per immobilization method (color coded) and the background spectrum (mean plus tripled standard deviation of 25 empty PCR cup measurements displayed as gray solid line with gray area).

(h)) and 29th harmonic (synthetic cotton, s. Fig. 5(g)) onward. These observations are also valid, but less pronounced for the COOH spectra (SI Fig. S1), whereas the NH2 spectra show no clear differentiation (SI Fig. S2).

3.2.3. Influence of immobilization method on MPS parameters. Fig. 7 shows the MPS parameters A_3^*, A_5/A_3 and ϕ_3 for all samples with COOH, NH2 and plain particles. Additionally, the mean values and CVs can be found in Table 5.

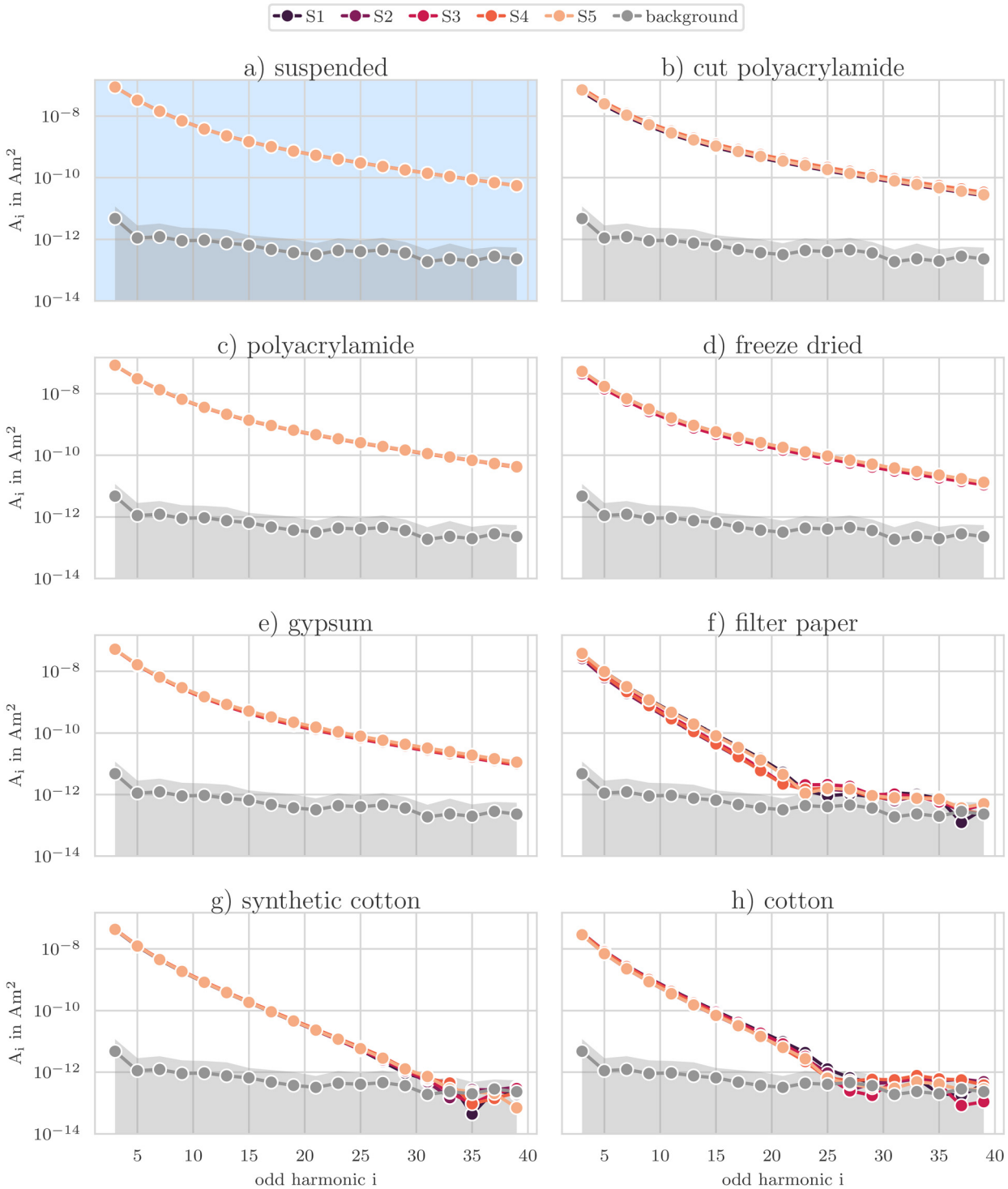

Fig. 6 MPS spectra of perimag® plain MNP for different immobilization methods. Shown are the odd harmonics for five replicate samples per immobilization method (color coded) and the background spectrum (mean plus tripled standard deviation of 25 empty PCR cup measurements displayed as gray solid line with gray area).

MNP amount dependent parameter A_3^*. For all MNP systems, A_3^* is highest for suspended samples and reduced whenever MNP are immobilized (s. Fig. 7 top panel). For COOH and plain particles, the smallest reduction of this parameter is found for polymerization-based immobilization followed by crystallization-based immobilization. The largest reduction in A_3^* is obtained for evaporation-based samples. When NH2 particles are considered, A_3^* differs significantly less between sus-

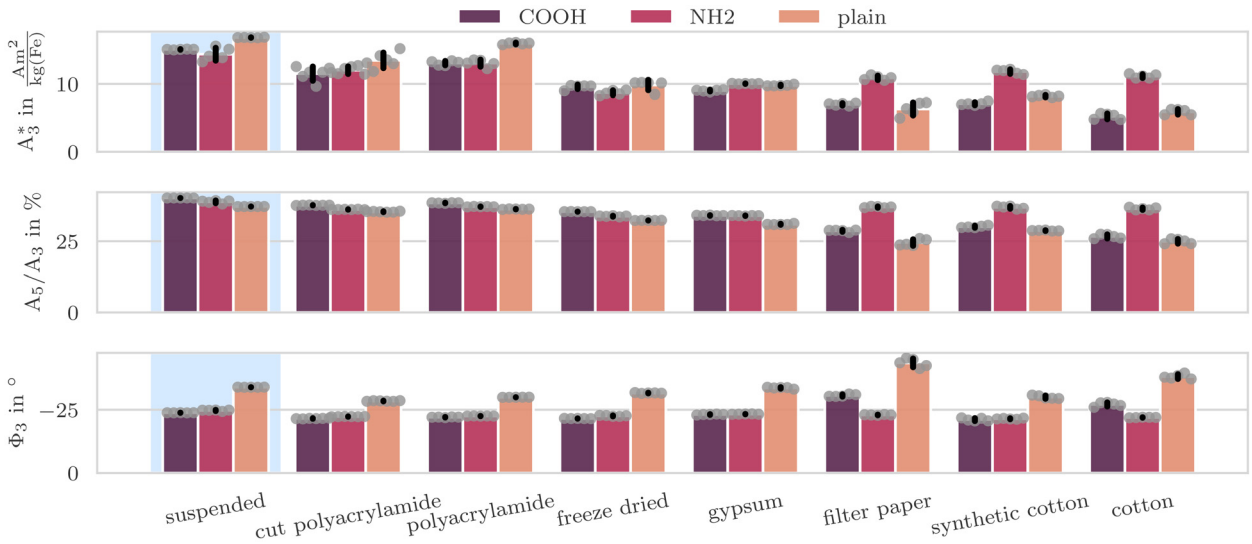

Fig. 7 Characteristic MPS signal parameters for three perimag® systems (COOH, NH2, plain) immobilized with different immobilization methods. Mean values (bar height) and standard deviations (black errorbar) were computed from the results for similarly prepared replicas for each immobilization method (shown as gray dots per bar). MNP in distilled water is included for comparison (suspended, leftmost).

Table 5 Mean values and coefficients of variation (CV) of characteristic MPS signal parameters for three perimag® systems (COOH, NH2, plain) immobilized with different immobilization methods; MNP in distilled water is included for comparison (suspended)

Immobilization method	MNP system	A_3^* mean (Am^2 $kg(Fe)^{-1}$)	A_3^* CV (%)	A_5/A_3 mean (%)	A_5/A_3 CV (%)	ϕ_3 mean (°)	ϕ_3 CV (%)
Suspended	COOH	15.10	0.29	40.25	0.027	−23.81	0.13
	NH2	14.4	6.6	38.9	1.2	−24.7	0.93
	Plain	16.85	0.19	37.23	0.040	−33.94	0.083
Cut polyacrylamide	COOH	12	9.1	37.68	0.16	−21.5	0.53
	NH2	12.0	4.6	36.20	0.17	−22.28	0.27
	Plain	13	8.5	35.4	0.40	−28.5	0.46
Polyacrylamide	COOH	13.1	2.4	38.50	0.24	−22.0	0.49
	NH2	13.1	4.0	37.17	0.19	−22.49	0.17
	Plain	16.0	0.80	36.31	0.19	−29.94	0.087
Freeze dried	COOH	9.6	3.4	35.43	0.076	−21.52	0.21
	NH2	8.7	3.9	33.8	0.48	−22.6	0.80
	Plain	9.8	7.7	32.33	0.090	−31.6	0.41
Gypsum	COOH	9.0	1.3	34.1	0.28	−23.1	0.61
	NH2	10.04	0.35	34.00	0.23	−23.26	0.29
	Plain	9.8	1.0	31.0	0.57	−33.7	0.87
Filter paper	COOH	7.0	2.6	28.7	1.2	−30.7	1.4
	NH2	10.9	3.0	37.0	0.61	−22.9	0.57
	Plain	6.3	15	25	4.7	−44	3.9
Synthetic cotton	COOH	7.1	3.2	30.1	1.2	−21.1	2.7
	NH2	11.8	2.8	36.9	1.3	−21.42	0.88
	Plain	8.2	1.9	28.8	0.48	−30.0	2.1
Cotton	COOH	5.3	8.1	26.7	2.7	−27.1	2.9
	NH2	11.2	2.6	36.5	1.2	−21.93	0.40
	Plain	5.9	6.8	25.0	3.3	−38.2	2.4

pended and immobilized samples and among immobilization methods. Here, the lowest A_3^* reduction is again found for polyacrylamide immobilization but the largest reduction is observed for freeze dried samples followed by gypsum samples. When comparing the mean A_3^* values for the three systems within the immobilization methods, NH2 particles show the highest mean A_3^* values for evaporation-based methods, whereas for polyacrylamide and crystallization-based methods, very similar or only slightly lower mean A_3^* values are observed than for the other systems. The normalized third harmonic $\tilde{A}_3^*$ of the cut polyacrylamide samples increases for pieces from the top slice to the bottom slice for all tested MNP systems (by 12–13% for coated MNP and by 23% for plain) (SI Fig. S3).

MNP amount independent parameters A_5/A_3 and Φ_3. The A_5/A_3 ratio is highest when MNP are in suspended state, where the highest value is achieved for COOH and the lowest value for plain samples (s. Fig. 7 middle panel). This trend remains

unchanged after immobilization with polymerization-based and crystallization-based methods with only a small decrease in the single values. For evaporation based immobilization, further reduced A_5/A_3 values are found for COOH and plain, whereas NH2 remains in the same range as for the other methods. Whereas Φ_3 values are comparable to the respective suspended samples for polymerization, crystallization and synthetic cotton immobilization, significantly increased values can be observed for COOH and plain MNP with filter paper and cotton immobilization (s. Fig. 7 bottom panel). In case of NH2, Φ_3 remains in the same range for all immobilization materials. Both MNP amount independent MPS parameters do not show any trend in dependence of cutting site within the batch.

3.2.4. Reproducibility of magnetic properties within immobilization method. By measuring a polyacrylamide sample six times, the procedural uncertainty as CV of the MPS was assessed to be 0.080% for A_3^*, 0.065% for A_5/A_3 and 0.21% for Φ_3.

When considering the COOH and plain MNP system, the variation of A_3^* is lowest for suspended samples and slightly increased for gypsum and polyacrylamide samples (*cf.* Fig. 7 top panel, Table 5). The low variability of A_3^* for these immobilization methods is also reflected in the MPS spectra, which show no significant amplitude and shape variation (*cf.* Fig. 6(a)–(c) and (e)). Apart from one outlier for both MNP systems, low variability is also found for freeze dried samples (outlier-eliminated CV < 1%). For COOH and plain MNP embedded in evaporation-based immobilization materials and cut polyacrylamide, A_3^* varies significantly with the highest variation for cut polyacrylamide (COOH) and filter paper (plain). In accordance, the MPS spectra show high amplitude and shape variability for these immobilization methods (*cf.* Fig. 6(f)–(h)). In contrast, NH2 particles exhibit the highest A_3^* variation when in suspended state or embedded in cut polyacrylamide and the clearly lowest variation for gypsum.

The MNP amount independent parameters A_5/A_3 and ϕ_3 vary significantly less than A_3^* for all immobilization methods (*cf.* Fig. 7 middle and bottom panel, Table 5). For COOH and plain particles, the overall minimal variation is obtained when MNP are in suspended state. Among the immobilized samples, only the A_5/A_3 and ϕ_3 variations for evaporation-based immobilization materials are noticeably high, with the most variation for cotton (COOH) and filter paper (plain), respectively. For NH2 samples, in contrast, a remarkably high variation in A_5/A_3 and Φ_3 is observed for suspended MNP, and among the immobilized samples for (synthetic) cotton (A_5/A_3) as well as for freeze dried and synthetic cotton (Φ_3).

3.3. MRX analysis

3.3.1. Influence of immobilization method on MRX relaxation signal. Exemplary, Fig. 8 presents the fitted relaxation signals of differently immobilized plain reference samples. The relaxation curves of the gypsum samples have the highest magnetic flux density at t_1 and the steepest drop to t_2 (s. Fig. 8(e)), followed by the freeze dried and polymerization-based samples (*cf.* Fig. 8(b)–(d)). Evaporation-based immobilization methods lead to considerably flatter relaxation signals and about half the magnetic flux densities at t_1 (*cf.* Fig. 8(f)–(h)). Compared to immobilized MNP, the relaxation curves for suspended particles show a substantially reduced magnetic flux density at t_1 and much flatter curves from t_1 onward (s. Fig. 8(a)). See SI Fig. S4 and S5 for the relaxation curves with COOH and HN2 MNP, respectively.

When evaluating the results of the MRX measurements, the choice of the time window considerably influences the extracted parameters. The parameters chosen in this study were determined based on previous experiments with immobilized particles. Depending on the actual particle properties, this window might not be optimal to reflect the complete relaxation process. For example, the relaxation of suspended particles, which is dominated by Brown relaxation, is almost completed at the beginning of the measurement window (s. Fig. 8a).

3.3.2. Influence of immobilization method on MRX parameters. Fig. 9 shows the MRX parameters ΔB, $t_{1/e}$ and IRT for all suspended and immobilized samples with COOH, NH2 and plain particles. The mean values and CVs can be found in numerical form in Table 6.

MNP amount dependent parameter ΔB. For all investigated MNP systems, the relaxation amplitude is lowest for suspended samples, with NH2 showing the highest ΔB value among the systems (s. Fig. 9 top panel). Compared to suspended, significantly higher relaxation amplitudes are observed for the immobilized samples for all MNP systems. For evaporation-based immobilization methods, NH2 retains the highest value among the MNP systems, whereas the plain system shows the highest ΔB for crystallization-based and polymerization-based immobilization. With COOH and plain particles, the highest relaxation amplitudes are obtained for gypsum, followed by cut polyacrylamide and freeze dried samples. With NH2, ΔB is maximal for evaporation-based samples. The lowest relaxation amplitudes are exhibited for polyacrylamide and synthetic cotton in case of COOH, for evaporation-based samples in case of plain MNP and for freeze dried samples in case of NH2 MNP. The normalized parameter $\widetilde{\Delta B}$ for the cut polyacrylamide samples increases slightly from upper to lower batch slices is observed for the coated MNP systems (8.8% for COOH, 9.6% for NH2) and a significantly stronger or the plain system (26%) (SI Fig. S6).

MNP amount independent parameters $t_{1/e}$ and IRT. As with ΔB, the relaxation time $t_{1/e}$ is lowest for suspended samples in all MNP systems with considerably higher values for NH2 samples compared to plain and COOH (s. Fig. 9 middle panel). For plain particles, $t_{1/e}$ increases strongly for all immobilization materials where polyacrylamide immobilization is the only method that leads to a noticeably shorter relaxation time. For NH2 particles, too, only the relaxation times of polyacrylamide and cut polyacrylamide samples can be distinguished from the others. For COOH particles, similar relaxation times are obtained for evaporation-based and gypsum samples, whereas shorter relaxation times are observed for freeze dried and polymerization-based samples. Unlike $t_{1/e}$, the

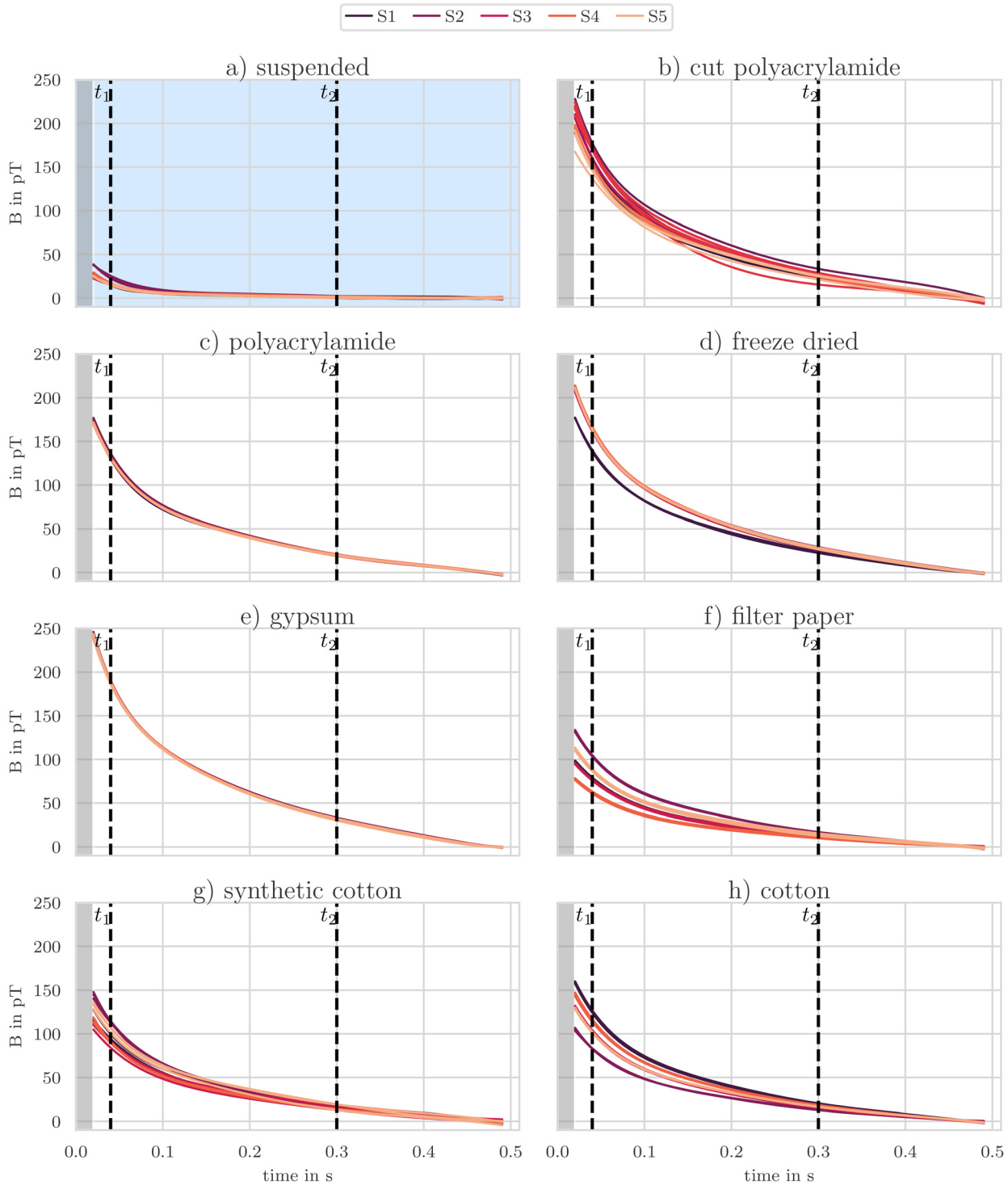

Fig. 8 MRX signals of perimag® plain MNP for different immobilization methods. Shown are fitted relaxation signals for five replicate samples per immobilization method (color coded). MNP in distilled water is included for comparison (suspended, leftmost). The excitation field is turned off at t = 0 ms. The dashed vertical black lines indicate the time points t_1 = 40 ms and t_2 = 300 ms used to determine the MRX parameters. The beginning of the measurement signal contains a short section after the excitation current is switched off, which is not evaluated, for example due to switching effects (dead time, gray background).

integral relaxation time does not differ significantly between all MNP systems and immobilization methods (s. Fig. 9 bottom panel). Whereas $t_{1/e}$ and IRT of immobilized samples yield very similar values among the three tested MNP systems, suspended samples reveal significant differences between the systems. The MNP amount independent MRX parameters do

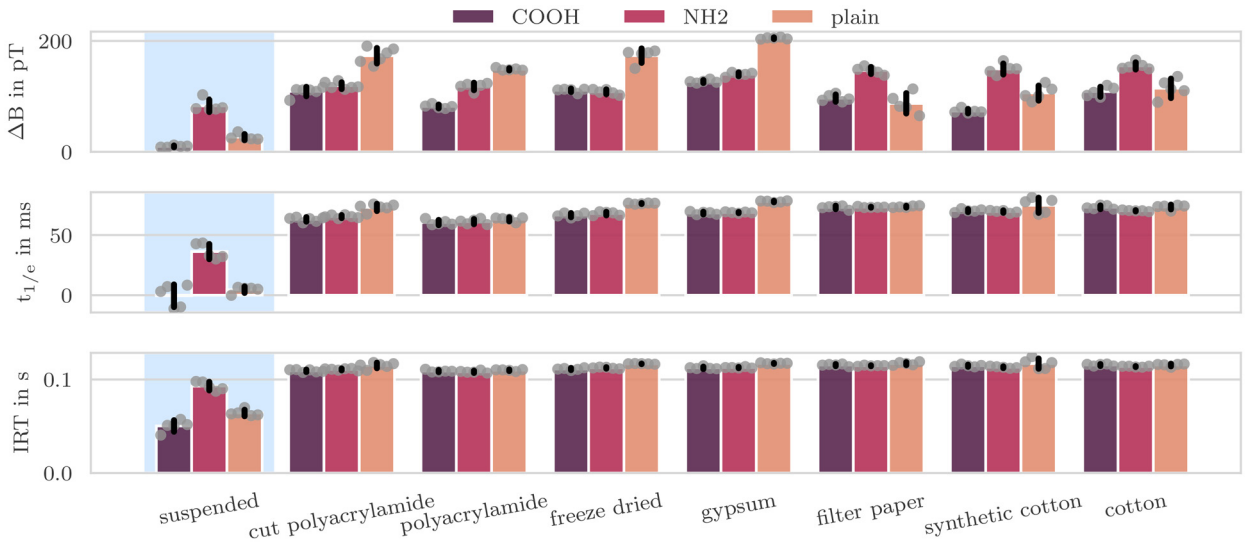

Fig. 9 Characteristic MRX signal parameters for three perimag® systems (COOH, NH2, plain) immobilized with different immobilization methods. Mean values (bar height) and standard deviations (black errorbar) were computed from the results for similarly prepared replicas for each immobilization method (shown as gray dots per bar). MNP in distilled water is included for comparison (suspended, leftmost).

Table 6 Mean values and coefficients of variation (CV) of characteristic MRX signal parameters for three perimag® systems (COOH, NH2, plain) immobilized with different immobilization methods; MNP in distilled water is included for comparison (suspended)

Immobilization method	MNP system	ΔB mean (pT)	ΔB CV (%)	$t_{1/e}$ mean (ms)	$t_{1/e}$ CV (%)	IRT mean (s)	IRT CV (%)
Suspended	COOH	10	14	2	258	0.05	19
	NH2	83	13	36	17	0.093	4.9
	Plain	27	20	5	51	0.064	7.1
Cut polyacrylamide	COOH	109	7.5	63	2.9	0.109	1.2
	NH2	119	5.1	65	1.9	0.111	0.90
	Plain	173	8.0	73	4.1	0.115	2.6
Polyacrylamide	COOH	82	4.1	60	3.5	0.109	1.1
	NH2	118	5.7	61	3.5	0.108	1.1
	Plain	149	1.4	63	2.7	0.1099	0.8
Freeze dried	COOH	111	2.9	67	2.6	0.111	1.0
	NH2	108	4.0	68	2.2	0.1125	0.68
	Plain	173	7.7	76.4	0.44	0.1169	0.39
Gypsum	COOH	127	2.1	68	1.7	0.113	1.1
	NH2	140	2.4	68.8	0.73	0.1128	0.57
	Plain	205	0.76	78.0	0.79	0.1173	0.41
Filter paper	COOH	97	6.7	73	2.0	0.116	1.2
	NH2	146	4.2	73.3	0.49	0.1149	0.56
	Plain	88	21	73.7	0.97	0.117	1.4
Synthetic cotton	COOH	74	5.4	70	1.8	0.115	1.0
	NH2	149	6.6	70	1.5	0.1132	0.81
	Plain	106	13	75	8.4	0.117	4.6
Cotton	COOH	108	8.1	73	2.1	0.116	1.0
	NH2	155	4.2	70.3	0.74	0.1139	0.46
	Plain	115	15	73	2.7	0.116	1.2

not show a dependence on the cutting site for cut polyacrylamide samples within the batch.

3.3.3. Reproducibility of magnetic properties within immobilization method. The procedural uncertainty of MRX in form of CV was determined to be 0.75% for ΔB, 0.94% for $t_{1/e}$ and 0.27% for IRT by a sixfold measurement of a single polyacrylamide sample with plain MNP (*cf.* Fig. 1).

For all investigated MNP systems, ΔB varies most for suspended samples (*cf.* Fig. 9 top panel, Table 6). For plain MNP, the filter paper samples yield a similar variation, followed by the other two evaporation-based methods. For COOH, evaporation-based methods, together with cut polyacrylamide, also show higher variability in the relaxation amplitude compared to other types of immobilization. For NH2 particles, the ΔB variability is highest for synthetic cotton compared to a slightly reduced variability for the other immobilization methods. In all MNP systems, the least ΔB variation is obtained for freeze dried samples (plain CV 1.2% without outlier) or MNP in

gypsum. The variability of the relaxation amplitude is also reflected in the MRX relaxation signals (*cf.* Fig. 8), where *e.g.* the relaxation signals for plain particles immobilized with gypsum, freeze drying (with one outlier) and polyacrylamide are very congruent (*cf.* Fig. 8(c)–(e)), whereas the relaxation curves for the cut polyacrylamide and evaporation-based immobilized samples vary considerably (*cf.* Fig. 8(b), (f)–(h)). In all examined combinations of immobilization material and MNP system, the variability of relaxation signals is reflected in fluctuations in signal steepness rather than in offset shifts. By normalizing ΔB to the sample weight for the cut polyacrylamide samples, the variability is reduced by half for COOH particles and by one third for NH2 particles (*cf.* SI Fig. S6). This effect cannot be observed for plain particles.

As with ΔB, $t_{1/e}$ varies most for the suspended samples, regardless of the MNP system used (*cf.* Fig. 9 middle panel, Table 6). The CVs for the MNP amount independent relaxation time are even higher than for the MNP amount dependent relaxation amplitude and show a clear outlier for suspended COOH. Among immobilized samples, $t_{1/e}$ exhibits low variation for crystallization-based samples (all MNP systems) and cotton (COOH, NH2), whereas higher $t_{1/e}$ variation is observed for polyacrylamide (all systems) and cotton (plain). The highest variability of IRT is also observed for suspended samples, however the overall variability is lower compared to $t_{1/e}$ variability (*cf.* Fig. 9 middle and bottom panel, Table 6). For COOH, IRT varies to similar extent for all immobilization methods with slightly increased variability for cut polyacrylamide and filter paper samples. For plain, the IRT CVs of the immobilization methods differ more clearly, with the maximum for cut polyacrylamide and the minimum for crystallization-based samples. In contrast, NH2 MNP lead to the lowest IRT variation for cotton samples and the highest variation when embedded in polymerization-based materials.

4. Discussion

4.1. Influence of immobilization method on magnetic properties

Compared to suspended MNP, immobilized MNP of all immobilization materials and MNP systems show a signal drop in the MPS spectrum and parameters, as well as steeper relaxation curves and increased MRX parameters (*cf.* Fig. 6–9). Taking into account the chosen MRX window, both modalities reflect the typical and well-known immobilization-related changes.[18,37,48] This confirms the fundamental suitability of the examined materials for immobilizing MNP with different surface coatings.

However, the specific manifestation of the immobilization-induced changes in dynamic and static magnetic properties varies among immobilization materials, with the underlying immobilization mechanism being the most influential factor (*cf.* Fig. 7 and 9). Immobilization methods based on the same mechanism, *i.e.* water evaporation for cotton, synthetic cotton and filter paper, crystallization for gypsum and freeze drying, and polymerization for (cut) polyacrylamide, tend to exhibit more similar magnetic properties. Meanwhile, immobilization methods incorporating different underlying mechanisms, *e.g.* filter paper and freeze drying, led to significantly different manifestations of magnetic properties. Depending on the mechanism, the immobilization process leads to different MNP arrangements with potential aggregation in the immobilization material and triggers different reactions of the MNP with the immobilization material. The extent to which the results of samples from different immobilization groups are similar depends on the surface coating of the MNP used (*cf.* section 4.3) and on whether dynamic magnetic properties (*e.g. via* MPS) or static properties (*e.g. via* MRX) are investigated.

For each modality, the differences between immobilization methods are significantly more pronounced for MNP amount dependent properties than for their MNP amount independent counterparts (*e.g.* Fig. 7 top panel *vs.* middle and bottom panel). Whereas the differences in MNP amount dependent quantities are influenced by both the type of immobilization and effects related to the specific iron amount in the sample, MNP amount independent quantities provide valuable information about MNP mobility and interaction with the direct environment of the MNP.[14,43,49,50] The observed differences in the MNP amount independent MPS parameter A_5/A_3 (s. Fig. 7 middle panel) suggest that different types of MNP embedding cause distinguishable dynamic magnetic properties of the samples. On the other hand, the static MNP amount independent properties examined with MRX appear to be rather independent of the immobilization material (s. Fig. 9 middle and bottom panel). For meaningful initial experiments that are application-related, the choice of the immobilization material is particularly relevant, because most established MNP application scenarios, such as MPI, MRX imaging *etc.*, are based on quantifying iron content resulting into the necessity to investigate MNP amount dependent sample properties.

If polyacrylamide samples are produced in such a way that polymerization takes place in batches from which pieces are subsequently cut out, the MNP amount dependent parameters depend on the cutting site within the batch. Due to parameters that indicate higher iron amount for deeper batch slices, it is likely that MNP sink down in the rather loose polymer matrix of the batch. Whether this effect occurs depends primarily on the combination of the mesh size and the hydrodynamic diameter of the MNP[31] as well as on the surface coating. Dependence on the cutting site can be prevented to a certain extent by polymerizing the target amount of MNP-loaded hydrogel directly in the target container. Optical methods can be used to verify the homogeneity of MNP in hydrogels and provide helpful insights into polymer mesh density and possible MNP aggregation in the matrix.[31] A careful choice of MNP type and polyacrylamide properties is necessary to achieve reliable homogeneous embedding of MNP in polymer matrices.

The contributions of the control samples to the MPS spectra suggest that gypsum contains varying amounts of magnetic impurities (*cf.* Fig. 5(d)). Pure gypsum, as a calcium

sulfate mineral, should be non magnetic. Commercially available gypsum powder, as used in most practical immobilization studies and also here, usually contains not only calcium sulfates but also magnetic impurities resulting from the production process. However, to the best of our knowledge, the origin of these impurities has not been investigated in detail. The same applies to a lesser extent to filter paper (*cf.* Fig. 5(e)) made from recycled paper with possible residues of printer ink. The small magnetic background signal for filter paper was also reported in Hashimoto *et al.*[22] This type of magnetic contamination cannot be prevented, but is only of importance if samples with very small iron amounts are examined. Since the MPS amplitudes of the gypsum and filter paper control samples observed here are orders of magnitude lower than the signals of corresponding samples with MNP (10^{-9} Am^2 compared to 10^{-7} Am^2, *cf.* Fig. 5(d), (e) and 6(e), (f)), the magnetic impurities do not enter the MNP amount dependent parameter A_3^* for the investigated iron concentration.

As MPI and MRXI are directly derived from the measurement principles MPS and MRX used in this study, insights are transferrable to both imaging methods and a direct influence of the immobilization method on the imaging results is assumed.

4.2. Reproducibility of magnetic properties within immobilization method

The reproducibility of magnetic properties within an immobilization method allows an assessment of the precision with which magnetic properties can be defined *via* MNP immobilization and thus represents an important quality criterion. For the reproducibility, the underlying mechanism of immobilization plays a role, whereby immobilization methods of the same group (polymerization, crystallization and evaporation) tend to cause similar variability for static and dynamic magnetic properties (*cf.* Fig. 7, 9 and Tables 5, 6). However, the distinction between the three groups is less clear for the variability of the properties than for the properties themselves. Evaporation-based immobilization methods stand out with low reproducibility for almost all parameters and MNP systems examined, especially for neutral (plain) and negatively charged (COOH) MNP systems. This group of immobilization methods is characterized by an increased probability of particle–particle interactions, as evaporation leads to a relatively uncontrolled rearrangement of the MNP from 3D in the suspended state to 2D on the surface of the immobilization materials' fibers. The sample-specific rearrangement leads to an increased proximity of MNP on the fibers, resulting in sample-specific interactions that increase the variability of magnetic properties among replicas. Compared to evaporation-based methods, immobilization mechanisms that impose more controlled MNP arrangements, *e.g.* by "freeze drying" the MNP into a sugar crystal matrix, lead to more similar MNP arrangements among replicas and thus to higher reproducibility of the magnetic properties.

As expected, MNP amount dependent properties vary almost always considerably more than properties that are independent from the MNP amount of the sample (*e.g.* Fig. 7 top *vs.* middle and bottom panel) because of the reduced influence of preparation uncertainties. Whereas the variability of MNP amount dependent properties lies clearly above the procedural uncertainty of the respective modality for all immobilization methods, the variations of the MNP amount independent quantities only differ clearly from the procedural uncertainty for evaporation-based immobilization (*cf.* sections 3.2.4, 3.3.3 and Tables 5, 6). This emphasizes that evaporation-based immobilization is inferior to other immobilization mechanisms in terms of the reproducibility of magnetic properties, even without taking iron content influences into account.

Particularly for MNP amount dependent properties, the preparation procedure represents another important factor for the reproducibility of magnetic sample properties. The example of polyacrylamide *versus* cut polyacrylamide clearly shows how much variability can be introduced by a change in the preparation method (*cf.* Fig. 7 top panel, Fig. 9 top panel), which in some circumstances cannot be compensated for, even by a normalization of MNP amount dependent parameters (s. SI Fig. S3 and S6). Please note that one batch for each of the three MNP dilutions was prepared and used for all replicas (except for polyacrylamide ones). Even greater variability in the MNP amount dependent parameters can be expected if the original stock solution and distilled water are pipetted consecutively into each phantom container. This means that careful planning of the exact immobilization procedure is essential for the adequate interpretation of results.

The level of reproducibility in magnetic properties for suspended samples and those immobilized with materials of the three groups is also closely linked to the coating of the investigated MNP system (s. section 4.3) and how which properties are captured (dynamic *vs.* static and parameter choice). For example, as expected, the dynamic magnetic properties determined using MPS are particularly stable for suspended non-negatively charged particles (s. Fig. 7). In contrast, a particularly high variability of the static magnetic properties for suspended samples is observed in the MRX (s. Fig. 9), which can be attributed to the relaxation being almost complete at the time point t_1 (as stated in section 3.3.1).

The investigation of replicas allows for the detection of material loss during sample preparation which is indicated by consistently lower MNP amount dependent MPS and MRX parameters compared to samples of the same set (*e.g.* plain freeze dried samples in Fig. 7 top panel). As expected, the material loss does not influence the MNP amount independent parameters. For MRX, outliers for suspended samples can appear due to insufficient fitting quality. Here, the almost completed relaxation process causes a flat relaxation signal for which the OMP dictionary is not optimized (*cf.* Table 6 suspended COOH).

4.3. On the role of surface functionalization

The characterization of the MNP stock solutions confirms similar magnetic properties of the cores and structural similarities of the MNP in general, therefore differences between

MNP systems can be attributed mainly to surface differences, *i.e.* differences in the effective electric charge of the MNP surfaces. In this context, the results for the positively charged NH2 system should be interpreted with caution due to several reasons. Difficulties in pipetting were encountered for the surface coated MNP systems and preliminary experiments revealed signs of long-term stability issues with NH2. Additionally, aggregation of the suspended NH2 MNP is indicated by both the increased hydrodynamic diameter s. (Table 4) and the significantly slowed relaxation (*cf.* increased relaxation time in Fig. 9 and SI Fig. S5(a)). The NH2 aggregation might not be reflected in the PDI values, because the DLS measurement was performed immediately after the preparation of the MNP dilution, before aggregation and long-term instability came into play.

Despite this limitation, it can be recognized that the surface functionalization strongly determines how clearly the three mechanism-based groups of immobilization methods can be distinguished, both for the magnetic properties themselves and for their reproducibility. Whereas the three groups can be clearly distinguished for particles with an uncharged surface, the differences are less pronounced for negatively charged MNP and almost non-existent for positively charged MNP (*cf.* Fig. 7 and 9). This behavior is unexpected since it was assumed that loaded MNP would differentiate immobilization materials more clearly due to different conceivable combinations of the MNP charge and the charge of the immobilization material.

The surface functionalization has a greater impact on the MNP amount dependent magnetic properties compared to the MNP amount independent ones, especially when static properties are investigated (*e.g.* Fig. 9 top *vs.* middle and bottom panel).

Also remarkable is the interplay of the immobilization method group and the surface coating with respect to MNP amount dependent quantities. Here, crystallization-based and polymerization-based immobilization maintains the relations of absolute MPS parameter values between the MNP systems compared to suspended samples, whereas evaporation-based immobilization modifies the relation of the absolute MPS parameters for the three MNP systems (*cf.* Fig. 7 top panel). For the MNP amount dependent MRX parameter, the opposite picture emerges, whereby the relationship between relaxation amplitudes for suspended samples remains unchanged for evaporation-based methods but differs for crystallization and polymerization-based methods (*cf.* Fig. 9 top panel).

4.4. On the practicality of MNP immobilization procedures

In addition to the measurable magnetic properties, the practicality of the MNP immobilization procedure is of particular importance for the choice of the immobilization method (s. Table 3).

In terms of the time required for complete sample production, the immobilization material gypsum is particularly advantageous, thanks to its short preparation and hardening times. If a longer waiting time until complete immobilization can be tolerated, freeze drying, cotton wool or filter paper are also acceptable options, although the aforementioned rather undefined and less reproducible immobilization process associated with evaporation-based methods must be taken into account (*cf.* section 4.2). Although hydrogels require a relatively short time to polymerize completely, they require by far the most preparation steps, resulting in a higher susceptibility to inaccuracies.

Whereas immobilization with gypsum and evaporation-based methods only requires basic equipment, more specialized laboratory equipment (ice bath, fume hood, reagents) is required for immobilization with polyacrylamide, and freeze drying is only possible with the corresponding device. Other hydrogels, such as agarose or gelatine, require fewer reagents, but usually still need water baths and a multi-step procedure. All investigated immobilization materials are harmless to health, with the exception of the polyacrylamide components Tetramethylethylenediamine and Acrylamide (toxic) that must be handled with caution.

Whenever preliminary studies for clinical applications of MNP are to be conducted, the similarity of the sample to human tissue is another important criterion. Among the tested immobilization materials, hydrogels such as polyacrylamide can be considered more similar to human tissue due to their high water content and the resulting softer consistency. Nevertheless, the other immobilization materials tested could also adequately mimic specific properties of MNP-loaded tissue, although this cannot be assessed on the basis of this study with non-biological immobilization methods only.

4.5. Recommendations

The results of this study are valid for the experimental conditions considered here (immobilization procedures, material selection, particle systems, measurement modalities *etc.*). Deviations are to be expected for other conditions. The best immobilization method depends on the objective of the planned study and the available time and resources. Nevertheless, a number of recommendations can be derived based on the findings obtained here (see Table 7 for an overview of the qualitative performance of the immobilization methods regarding the discussed aspects). For fast and reliable immobilization of MNP, gypsum can be recommended as it has the shortest preparation time, low variability in magnetic properties for various MNP systems and does not require any special laboratory equipment. If hydrogels are used due to their greater similarity to tissue, a homogeneous MNP distribution in the polymer matrix needs to be verified. The polymerization in the target vessel is clearly preferable to cutting hydrogel pieces from an already polymerized batch. Whenever small amounts of iron or small changes in magnetic properties, particularly those dependent on MNP quantities, are investigated, the influence of possible magnetic impurities in the immobilization materials must be checked and replicas should be prepared. The use of evaporation-based immobilization methods is not recommended, especially for studies with a single sample, as the possible chaotic rearrangement of MNP

Table 7 Qualitative comparison of the MNP immobilization methods (for each characteristic, the best performing method is highlighted in bold)

	Immobilization method				
Characteristic	Polyacrylamide	Freeze drying	Gypsum	Filter paper	(Synthetic) cotton
Preparation practicality	Low	Medium	**High**	Medium	Medium
Preparation costs	High	Medium	**Low**	**Low**	**Low**
Level of MNP rearrangement	Medium	**Low**	**Low**	High	High
Magnetic contamination of immobilization material	**No**	**No**	Yes	Yes	**No**
Reproducibility of MNP amount dependent MPS parameters	Medium	**High**	**High**	Low	Low
Reproducibility of MNP amount independent MPS parameters	**High**	**High**	**High**	Medium	Medium
Reproducibility of MNP amount dependent MRX parameters	Medium	Medium	**High**	Low	Low
Reproducibility of MNP amount independent MRX parameters	Medium	Medium	**High**	**High**	**High**
Overall reproducibility	Medium	**High**	**High**	Low	Low

may have a greater effect on the magnetic properties than the characteristics being investigated. Because the specific MNP system used and the measurement modality influence the magnetic properties and reproducibility of the immobilized samples, it is advisable to use the particles and measurement procedures planned for the actual application even for early-stage experiments. Finally, the diversity and complexity of the factors influencing the magnetic properties of differently immobilized samples confirm that generalizations from one type of immobilization to immobilized MNP in general are not permissible.

5. Conclusions

The results demonstrate the importance of choosing the proper immobilization method to provide reliable and reproducible references with defined magnetic properties. Our findings give a clear recommendation to use controllable immobilization methods such as freeze drying and gypsum for immobilization of MNP. In contrast, evaporation-based methods tend to result in more unpredictable magnetic behavior of MNP mostly due to increased particle–particle interactions.

Finally, our procedure can be easily extended to other immobilization or embedding methods. Together with the two powerful magnetic characterization methods MPS and MRX, this provides an approach to find and compose appropriate references for the corresponding imaging modalities MPI and MRXI. As MPI and MRXI are directly derived from the measurement principles MPS and MRX used in this study, insights are transferrable to both imaging methods and a direct influence of the immobilization method on the imaging results is assumed. Future work will extend our approach to provide references with defined magnetic properties that describe MNP embedded in tissue for early-stage experiments.

Author contributions

Kerstin Pansegrau: conceptualization, data curation, formal analysis, investigation, methodology, software, validation, visualization, writing – original draft. Patricia Radon: data curation, investigation, validation, writing – review & editing. Aaron Jaufenthaler: validation, writing – review & editing. Frank Wiekhorst: conceptualization, funding acquisition, investigation, project administration, resources, supervision, validation, writing – review & editing. Daniel Baumgarten: conceptualization, funding acquisition, project administration, supervision, writing – review & editing.

Conflicts of interest

There are no conflicts to declare.

Data availability

The datasets generated and analyzed during the current study are available from the corresponding author on reasonable request.

Supplementary information (SI): besides the additional figures, we provide the aggregated MRX and MPS measurement data in CSV format. See DOI: https://doi.org/10.1039/d5nr05283a.

Acknowledgements

This research was funded in whole or in part by the Austrian Science Fund (FWF), grant 10.55776/PAT7880823 and is based upon work from COST Action CA23132 “Magnetic Particle Imaging for next-generation theranostics and medical research”(NexMPI), supported by COST (European Cooperation in Science and Technology). The PTB guest scientist program giving the opportunity for K. Pansegrau to carry out MRX and MPS experiments is kindly acknowledged.

References

1 J. K. Kirsch, *Top Magn. Reson. Imaging*, 1991, **3**, 1.
2 R. Weissleder, G. Elizondo, J. Wittenberg, A. S. Lee, L. Josephson and T. J. Brady, *Radiology*, 1990, **175**, 494–498.
3 B. Gleich and J. Weizenecker, *Nature*, 2005, **435**, 1214–1217.

4 J. Lange, R. Kötitz, A. Haller, L. Trahms, W. Semmler and W. Weitschies, *J. Magn. Magn. Mater.*, 2002, **252**, 381–383.
5 F. Wiekhorst, U. Steinhoff, D. Eberbeck and L. Trahms, *Pharm. Res.*, 2012, **29**, 1189–1202.
6 D. Baumgarten, M. Liehr, F. Wiekhorst, U. Steinhoff, P. Münster, L. Trahms and J. Haueisen, *Med. Biol. Eng. Comput.*, 2008, **46**, 1177–1185.
7 M. Liebl, U. Steinhoff, F. Wiekhorst, J. Haueisen and L. Trahms, *Phys. Med. Biol.*, 2014, **59**, 6607.
8 A. Jaufenthaler, T. Sander, P. Schier, K. Pansegrau, F. Wiekhorst and D. Baumgarten, *J. Magn. Magn. Mater.*, 2024, **596**, 171983.
9 A. S. Lübbe, C. Alexiou and C. Bergemann, *J. Surg. Res.*, 2001, **95**, 200–206.
10 Q. A. Pankhurst, J. Connolly, S. K. Jones and J. Dobson, *J. Phys. D: Appl. Phys.*, 2003, **36**, R167–R181.
11 J.-H. Lee, Y.-M. Huh, Y.-w. Jun, J.-w. Seo, J.-t. Jang, H.-T. Song, S. Kim, E.-J. Cho, H.-G. Yoon, J.-S. Suh and J. Cheon, *Nat. Med.*, 2007, **13**, 95–99.
12 H. Richter, M. Kettering, F. Wiekhorst, U. Steinhoff, I. Hilger and L. Trahms, *Phys. Med. Biol.*, 2010, **55**, 623.
13 S. Dutz, M. Kettering, I. Hilger, R. Müller and M. Zeisberger, *Nanotechnology*, 2011, **22**, 265102.
14 M. Liebl, F. Wiekhorst, D. Eberbeck, P. Radon, D. Gutkelch, D. Baumgarten, U. Steinhoff and L. Trahms, *Biomed. Tech.*, 2015, **60**, 427–443.
15 A. Jaufenthaler, V. Schultze, T. Scholtes, C. B. Schmidt, M. Handler, R. Stolz and D. Baumgarten, *EPJ Quantum Technol.*, 2020, **7**, 12.
16 P. Schier, M. Liebl, U. Steinhoff, F. Wiekhorst and D. Baumgarten, *Med. Phys.*, 2022, **49**, 3361–3374.
17 P. Schier, A. Jaufenthaler, M. Liebl, S. Arsalani, F. Wiekhorst and D. Baumgarten, *Phys. Med. Biol.*, 2023, **68**, 155002.
18 A. Remmo, D. Eberbeck, O. Kosch, L. Kampen, A. Ludwig, A.-N. Egler-Kemmerer, F. Wiekhorst and N. Loewa, *ACS Appl. Nano Mater.*, 2024, **7**, 24315–24324.
19 D. Eberbeck, F. Wiekhorst, U. Steinhoff and L. Trahms, *J. Phys.: Condens. Matter*, 2006, **18**, S2829–S2846.
20 S. Arsalani, P. Radon, P. Schier, A. Jaufenthaler, M. Liebl, D. Baumgarten and F. Wiekhorst, *Phys. Med. Biol.*, 2022, **67**, 225007.
21 P. Bender, J. Fock, C. Frandsen, M. F. Hansen, C. Balceris, F. Ludwig, O. Posth, E. Wetterskog, L. K. Bogart, P. Southern, W. Szczerba, L. Zeng, K. Witte, C. Grüttner, F. Westphal, D. Honecker, D. González-Alonso, L. Fernández Barquín and C. Johansson, *J. Phys. Chem. C*, 2018, **122**, 3068–3077.
22 S. Hashimoto, T. Oda, K. Yamada, M. Takagi, T. Enomoto, N. Ohkohchi, T. Takagi, T. Kanamori, H. Ikeda, H. Yanagihara, E. Kita and A. Tasaki, *Phys. Med. Biol.*, 2009, **54**, 2571–2583.
23 T. Yoshida, Y. Matsugi, N. Tsujimura, T. Sasayama, K. Enpuku, T. Viereck, M. Schilling and F. Ludwig, *J. Magn. Magn. Mater.*, 2017, **427**, 162–167.
24 M. A. A. Arenas, D. Gutkelch, O. Kosch, R. Brühl, F. Wiekhorst and N. Löwa, *Polymers*, 2022, **14**, 3925.
25 K. Everaert, T. Sander, R. Körber, N. Löwa, B. Van Waeyenberge, J. Leliaert and F. Wiekhorst, *Nanoscale Adv.*, 2023, **5**, 2341–2351.
26 P. Bender, A. Günther, A. Tschöpe and R. Birringer, *J. Magn. Magn. Mater.*, 2011, **323**, 2055–2063.
27 J. Wells, N. Löwa, H. Paysen, U. Steinhoff and F. Wiekhorst, *J. Magn. Magn. Mater.*, 2019, **475**, 421–428.
28 M. Salimi, W. Wang, S. Roux, G. Laurent, R. Bazzi, P. Goodwill, G. Liu and J. W. M. Bulte, *Nanoscale Adv.*, 2025, **7**, 1018–1029.
29 B. Gambin, P. Melnikova, E. Kruglenko, R. Strzałkowski and M. Krajewski, *J. Magn. Magn. Mater.*, 2022, **550**, 169000.
30 V. Zamora-Mora, P. Soares, C. Echeverria, R. Hernández and C. Mijangos, *Gels*, 2015, **1**, 69–80.
31 A. Shankar, A. P. Safronov, E. A. Mikhnevich, I. V. Beketov and G. V. Kurlyandskaya, *Soft Matter*, 2017, **13**, 3359–3372.
32 F. A. Blyakhman, A. P. Safronov, A. Y. Zubarev, T. F. Shklyar, O. G. Makeyev, E. B. Makarova, V. V. Melekhin, A. Larrañaga and G. V. Kurlyandskaya, *Results Phys.*, 2017, **7**, 3624–3633.
33 K. Kaczmarek, R. Mrówczyński, T. Hornowski, R. Bielas and A. Józefczak, *Nanomaterials*, 2019, **9**, 803.
34 L. Wöckel, J. Wells, O. Kosch, S. Lyer, C. Alexiou, C. Grüttner, F. Wiekhorst and S. Dutz, *J. Magn. Magn. Mater.*, 2019, **471**, 1–7.
35 R. Ludwig, M. Stapf, S. Dutz, R. Müller, U. Teichgräber and I. Hilger, *Nanoscale Res. Lett.*, 2014, **9**, 602.
36 A. Jaufenthaler, P. Schier, T. Middelmann, M. Liebl, F. Wiekhorst and D. Baumgarten, *Sensors*, 2020, **20**, 753.
37 S. Arsalani, P. Radon, D. Eberbeck, R. Körber, A. Jaufenthaler, D. Baumgarten and F. Wiekhorst, *Phys. Med. Biol.*, 2023, **68**, 175017.
38 N. Löwa, M. Seidel, P. Radon and F. Wiekhorst, *J. Magn. Magn. Mater.*, 2017, **427**, 133–138.
39 R. Kötitz, P. Fannin and L. Trahms, *J. Magn. Magn. Mater.*, 1995, **149**, 42–46.
40 R. W. Chantrell, S. R. Hoon and B. K. Tanner, *J. Magn. Magn. Mater.*, 1983, **38**, 133–141.
41 D. E. Koppel, *J. Chem. Phys.*, 1972, **57**, 4814–4820.
42 P. C. Fannin, B. Scaife and S. Charles, *J. Magn. Magn. Mater.*, 1988, **72**, 95–108.
43 N. Löwa, P. Knappe, F. Wiekhorst, D. Eberbeck, A. F. Thünemann and L. Trahms, *J. Magn. Magn. Mater.*, 2015, **380**, 266–270.
44 N. Löwa, L. Golusda, D. Paclik, H. Traub, M. Schannor, J. Saatz, C. Freise, M. Taupitz, B. Siegmund, A. A. Kühl and F. Wiekhorst, *Nanoscale Adv.*, 2025, **7**, 6525–6534.
45 R. Ackermann, F. Wiekhorst, A. Beck, D. Gutkelch, F. Ruede, A. Schnabel, U. Steinhoff, D. Drung, J. Beyer, C. Aßmann, L. Trahms, H. Koch, T. Schurig, R. Fischer, M. Bader, H. Ogata and H. Kado, *IEEE Trans. Appl. Supercond.*, 2007, **17**, 827–830.
46 F. Wiekhorst, C. Seliger, R. Jurgons, U. Steinhoff, D. Eberbeck, L. Trahms and C. Alexiou, *J. Nanosci. Nanotechnol.*, 2006, **6**, 3222–3225.

47 Y. Pati, R. Rezaiifar and P. Krishnaprasad, Proceedings of 27th Asilomar Conference on Signals, Systems and Computers, Pacific Grove, CA, USA, 1993, pp. 40–44.
48 D. Eberbeck, A. Khandhar, K. Krishnan and L. Trahms, 2015 5th International Workshop on Magnetic Particle Imaging (IWMPI), 2015, pp. 1–1.
49 E. Heim, M. Gerloff, F. Ludwig and M. Schilling, World Congress on Medical Physics and Biomedical Engineering, September 7–12, 2009, Munich, Germany, Berlin, Heidelberg, 2009, pp. 650–652.
50 A. Coene, J. Leliaert, M. Liebl, N. Löwa, U. Steinhoff, G. Crevecoeur, L. Dupré and F. Wiekhorst, *Phys. Med. Biol.*, 2017, **62**, 3139.